One-step synthesis of zerovalent-iron–biochar composites to activate persulfate for phenol degradation

Shu-hua Yao, Xue-jing Chen, Mario Alberto Gomez, Xi-chun Ma, Hai-bo Wang and Shu-yan Zang

ABSTRACT

A novel zerovalen-iron–biochar composite (nZVI/SBC) was synthesized by using $FeCl_3$-laden sorghum straw biomass as the raw material via a facile one-step pyrolysis method without additional chemical reactions (e.g., by $NaBH_4$ reduction or thermochemical reduction). The nZVI/SBC was successfully employed as an activator in phenol degradation by activated persulfate. XRD, SEM, N_2 adsorption–desorption and atomic absorption spectrophotometry analysis showed that the nanosized Fe^0 was the main component of the 4ZVI/SBC activator, which was a mesopore material with an optimal $FeCl_3{\cdot}6H_2O$/biomass impregnation mass ratio of 2.7 g/g. The 4ZVI/SBC activator showed an efficient degradation of phenol (95.65% for 30 min at 25 °C) with a large specific surface area of 78.669 $m^2{\cdot}g^{-1}$. The recovery of 4ZVI/SBC activator after the degradation reaction of phenol can be realized with the small amount of dissolved iron in the water. The 4ZVI/SBC activator facilitated the activation of persulfate to degrade phenol into non-toxic CO_2 and H_2O. The trend of Cl^-, SO_4^{2-} and NO_3^- affected the removal efficiency of phenol by using the 4ZVI/SBC activator in the following order: $NO_3^- > SO_4^{2-} > Cl^-$. The one-step synthesis of the nanosized zerovalent-iron–biochar composite was feasible and may be applied as an effective strategy for controlling organic waste (e.g. phenol) by waste biomass.

Key words | one-step method, phenol, sorghum straw, zerovalent-iron-biochar

Shu-hua Yao
Xue-jing Chen
Mario Alberto Gomez
Xi-chun Ma
Hai-bo Wang (corresponding author)
Shu-yan Zang
Liaoning Engineering Research Center for Treatment and Recycling of Industrially Discharged Heavy Metals,
Shenyang University of Chemical Technology,
Shenyang 110142, Liaoning,
China
E-mail: *wanghaibo@syuct.edu.cn*

Hai-bo Wang
College of Environmental and Safety Engineering,
Shenyang University of Chemical Technology,
Shenyang 110142,
China

INTRODUCTION

The recovery of water from wastewater is increasingly important for the sustainable development of the world due to the reduction of freshwater resources (Lei *et al.* 2015). The extensive use of phenol in different industrial processes has resulted in major water contamination problems, and phenol has been listed in the US EPA's list of priority pollutants (Lisowski *et al.* 2017). The activation of persulfate for the oxidation of phenol is regarded as an effective technology for phenol degradation in wastewater (Duan *et al.* 2018). However, persulfate is not able to degrade phenol without an activator (Lei *et al.* 2015). Thus it is imperative to develop low-cost, efficient and environmentally friendly activators for the activation of persulfate for phenol degradation. The activation of persulfate by iron (Kim *et al.* 2018) and related iron oxides (Yan *et al.* 2011) produces sulfate radicals ($SO_4^{\cdot-}$) (Fang *et al.* 2018) to degrade phenol, which is the most common activation process.

Iron and iron oxides have been extensively examined as reductants for treating various contaminants in water due to their strong redox potential (Hsueh *et al.* 2017), catalytic effects (Oh *et al.* 2017), low cost and naturally abundant material (Sun *et al.* 2012). Recently, research discoveries of iron and iron oxides activating persulfates to degrade phenol by using carbon nanotubes (Chen *et al.* 2007), nanodiamonds (Duan *et al.* 2016), and graphene (Lee *et al.* 2016; Wu *et al.* 2018) as supporters, have attracted unprecedented interest and inspired a myriad of studies of biochar as a sustainable catalyst for wastewater remediation (Huggins *et al.* 2016). Biochar derived from waste biomass is increasingly recognized as a multifunctional material for wastewater remediation applications due to biochar having the advantages of a feasible preparation method, low cost and abundant feedstocks (Wang *et al.* 2017). Several attempts have been made to develop upgraded biochar materials in

doi: 10.2166/wst.2020.001

combination with iron-bearing materials, such as biochar–Fe^0 composites and biochar–iron-oxide composites (Sun *et al.* 2012; Devi & Saroha 2014; Epold *et al.* 2015; Jung *et al.* 2016; Dong *et al.* 2017) due to the fact that biochar materials show good performance in dispersing and stabilizing the nanoparticles (Zhou *et al.* 2014). In addition, biochar can provide a large surface area, porous structure, and abundant functional groups to adsorb organic pollutants on its surface, thus enhancing the performance of iron–biochar composites in environmental applications. However, the synthesis of zerovalent-iron–biochar composites is expensive due to additional chemical reactions (e.g., by $NaBH_4$ reduction or thermochemical reduction) (Su *et al.* 2013; Oh *et al.* 2017; Wang *et al.* 2017) that may occur after pyrolysis of biochar, which is generally complex and time-consuming.

To avoid the cumbersome preparation and costly additional chemical reactions, one-step pyrolysis of $FeCl_3$-laden biomass was chosen to synthesize the zerovalent-iron–biochar composites in this work. Atomic absorption spectrophotometry, N_2 adsorption–desorption, SEM and XRD were used to characterize the synthesis activator for analysis of structural information and composition of the zerovalent-iron–biochar composites. The effects of iron content, activator dosage, phenol concentration, pH and inorganic ions on the activation of persulfate for phenol degradation were investigated. The oxidation results of phenol by the zerovalent-iron–biochar composite activators were also studied. Further, the mechanisms involved in the activation of persulfate for phenol degradation over the zerovalent-iron–biochar composites are further identified.

EXPERIMENTAL

Synthesis of the zerovalent-iron–biochar composites

The sorghum straw used in this work was collected locally in Shenyang, Liaoning Province, China. The sorghum straw was crushed with a powder machine to 0.125–0.177 mm and washed with deionized water four times to remove dirt, then dried at 80 °C. Sorghum straw powders (1 g) were firstly immersed into a $FeCl_3{\cdot}6H_2O$ solution at room temperature and the mixture was stirred for 24 h. After that, the solid residues were separated and put into a drying oven at 80 °C for 72 h. The $FeCl_3$-laden sorghum straw was pyrolyzed in a tube furnace at 800 °C under a nitrogen atmosphere for 2 h. The final composite products are denoted as nZVI/SBC. The $FeCl_3{\cdot}6H_2O$/biomass impregnation mass ratios of the final products used were 0.4 g/g for 1ZVI/SBC, 0.7 g/g for 2ZVI/SBC, 1.35 g/g for 3ZVI/SBC, 2.7 g/g for 4ZVI/SBC, 13.5 g/g for 5ZVI/SBC and 27 g/g for 6ZVI/SBC, respectively. The sorghum straw biochar (SBC) was produced by the pyrolysis of sorghum straw without the loading of $FeCl_3{\cdot}6H_2O$.

Characterization of the zerovalent-iron–biochar composites

Atomic absorption spectrophotometry (AA-6880) was used to detect the composition of nZVI/SBC and the concentration of iron. N_2 physical adsorption was carried out on a Micromeritics SSA-6000 volumetric adsorption analyzer to evaluate the Brunauer–Emmett–Teller (BET) surface area, the total pore volume, and pore diameters. A scanning electron microscope (SEM, Hitachi S-4800, Japan) was employed to analyze the morphology of SBC and 4ZVI/SBC. XRD (XRD-7000, Japan) analysis of nZVI/SBC was performed using a Rigaku X-ray diffractometer with Cu K_α radiation over 2 h with a collection range of 10°–80°. The absorbance of the samples was analyzed with an 1800PC spectrophotometer. The degradation of phenol was monitored by measuring the maximum absorbance at $\lambda = 510$ nm as a function of irradiation time.

Degradation of phenol

All experiments were conducted in solutions made from analytical grade chemicals and deionized water. Before degradation, 0.5 $g{\cdot}L^{-1}$ of SBC was added into 0.2 L of 0.025 $g{\cdot}L^{-1}$ phenol to examine the adsorption affinity of phenol without persulfate. Then a batch experiment of phenol degradation was carried out by adding persulfate under the previous conditions. To investigate the effect of $FeCl_3{\cdot}6H_2O$/biomass impregnation mass ratios on the activation of persulfate for phenol degradation, 0.5 $g{\cdot}L^{-1}$ of activators (nZVI/SBC with different $FeCl_3{\cdot}6H_2O$/biomass impregnation mass ratios of 0, 0.4, 0.7, 1.35, 2.7, 13.5 and 27 g/g) were added into 0.2 L of 0.025 $g{\cdot}L^{-1}$ phenol and 3.17 $g{\cdot}L^{-1}$ $Na_2S_2O_8$ aqueous solution (pH = 6.86) at 25 °C for 30 min. The effect of 4ZVI/SBC dosage (0.1, 0.2, 0.3, 0.4, 0.5 and 1.0 $g{\cdot}L^{-1}$) on the activation of persulfate for phenol degradation was observed in 0.2 L of 0.025 $g{\cdot}L^{-1}$ phenol and 3.17 $g{\cdot}L^{-1}$ $Na_2S_2O_8$ aqueous solution (pH = 6.86) at 25 °C for 30 min. The effect of inorganic ions (Cl^-, SO_4^{2-} and NO_3^-) on the activation of persulfate for phenol degradation was conducted by adding 0.5 $g{\cdot}L^{-1}$ 4ZVI/SBC activator in 0.2 L of 0.025 $g{\cdot}L^{-1}$ phenol and

3.17 g·L^{-1} $Na_2S_2O_8$ aqueous solution (pH = 6.86) at 25 °C for 30 min. The effect of phenol concentration (0.025, 0.05, 0.1 and 0.2 g·L^{-1}) on the activation of persulfate for phenol degradation was done by adding 0.5 g·L^{-1} 4ZVI/SBC activator in 3.17 g·L^{-1} $Na_2S_2O_8$ aqueous solution (pH = 6.86) at 25 °C for 30 min. The effect of pH (3.09, 5.04, 6.86, 9.06 and 11.03) on the activation of persulfate for phenol degradation was conducted by adding 0.5 g·L^{-1} 4ZVI/SBC activator in 0.2 L of 0.025 g·L^{-1} phenol and 3.17 g·L^{-1} $Na_2S_2O_8$ aqueous solution at 25 °C for 30 min. The chemical oxygen demand (COD_{Cr}) of the aqueous phase was confirmed in 0.025 g·L^{-1} phenol and 3.17 g·L^{-1} $Na_2S_2O_8$ aqueous solution (pH = 6.86) by adding 0.5 g·L^{-1} 4ZVI/SBC activator at 25 °C for 30 min.

RESULTS AND DISCUSSION

Effect of $FeCl_3·6H_2O$/biomass impregnation mass ratio on phenol degradation

The effect of different $FeCl_3·6H_2O$/biomass impregnation mass ratios on the activation of persulfate for phenol degradation is shown in Figure 1. Before the degradation experiment for phenol, SBC was used to investigate the adsorption affinity of phenol without persulfate. The adsorption removal rates of phenol were 2.9% for 10 min and 9.4% for 30 min, respectively. The results indicate that the adsorption effect of SBC was very low. This may be due to the fact that SBC had an adsorption affinity for phenol and the activation of persulfate for phenol degradation (Yang *et al.* 2011).

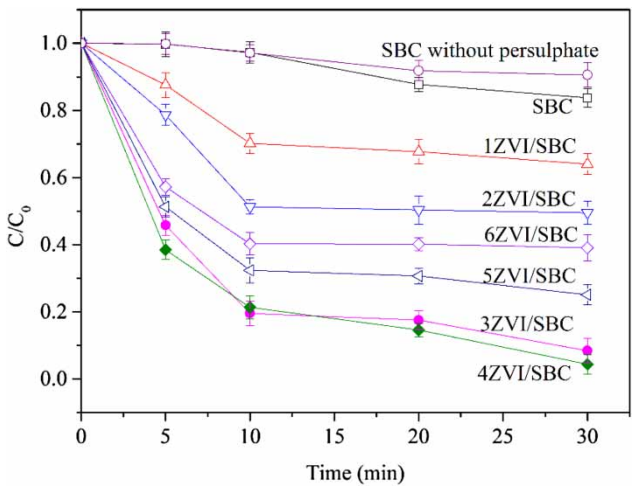

Figure 1 | Effect of different $FeCl_3·6H_2O$/biomass impregnation mass ratios on the activation of persulfate for phenol degradation.

A phenol removal of 16.30% was observed with the addition of 0.5 g·L^{-1} for the pure control SBC sample with persulfate. SBC reacted with persulfate as described in Equations (1) and (2) (Yang *et al.* 2011; Pu *et al.* 2014). The removal efficiency of phenol reached 35.99%, 50.48%, 91.60% and 95.65% for the activation of persulfate with 1ZVI/SBC, 2ZVI/SBC, 3ZVI/SBC and 4ZVI/SBC, respectively. The removal efficiency of phenol decreased from 95.65% with 4ZVI/SBC to 65.48% with 6ZVI/SBC. Noticeably, nZVI/SBC showed a better degradation performance of phenol than did SBC. The data strongly suggested that the removal efficiency of phenol was the highest (95.65%) when using 4ZVI/SBC as activator under the same conditions:

$$SBC_{surface} - OOH + S_2O_8^{2-} \rightarrow SBC_{surface} - OO^{\cdot} + SO_4^{\cdot-} + HSO_4^- \quad (1)$$

$$SBC_{surface} - OH + S_2O_8^{2-} \rightarrow SBC_{surface} - O^{\cdot} + SO_4^{\cdot-} + HSO_4^- \quad (2)$$

The microscopic morphological characteristics of SBC and 4ZVI/SBC were confirmed by SEM (Figure 2). The SBC had a relatively smooth surface and sheet structure, while 4ZVI/SBC had a rough surface adhered with some floccules. In order to obtain information about floccules distributed across the entire SBC surface, XRD was used to characterize the 4ZVI/SBC activator. XRD of nZVI/SBC with different $FeCl_3·6H_2O$/biomass impregnation mass ratios were obtained and is shown in Figure 3. In general, 1ZVI/SBC, 4ZVI/SBC, and 6ZVI/SBC exhibited the characteristic peak at $2\theta = 44°–45°$ assigned to Fe^0 (Wang *et al.* 2013), which is indicative of the presence of zerovalent iron on the iron–biochar composite. The characteristic peaks of FeOOH (Wang *et al.* 2013), $FeCl_2$ (Yang *et al.* 2016) and Fe_3O_4 (Huggins *et al.* 2016) were observed for the 6ZVI/SBC sample and the transformation of iron species during the pyrolysis process of calcining $FeCl_3$-laden sorghum straw could be explained by Equations (3)–(8) (Liu *et al.* 2013):

$$FeCl_3 + 3H_2O \rightarrow Fe(OH)_3 + 3HCl \quad (3)$$

$$Fe(OH)_3 \rightarrow FeO(OH) + H_2O \quad (4)$$

$$6FeO(OH) + H_2 \rightarrow 2Fe_3O_4 + 4H_2O \quad (5)$$

$$6FeO(OH) + CO \rightarrow 2Fe_3O_4 + CO_2 + 3H_2O \quad (6)$$

$$6FeO(OH) + C \rightarrow 2Fe_3O_4 + CO + 3H_2O \quad (7)$$

$$2FeCl_3 + H_2 \rightarrow 2FeCl_2 + 2HCl \quad (8)$$

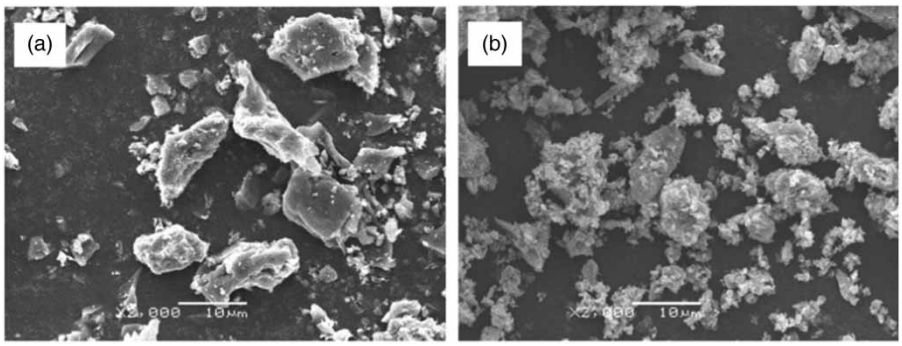

Figure 2 | SEM images of SBC and 4ZVI/SBC.

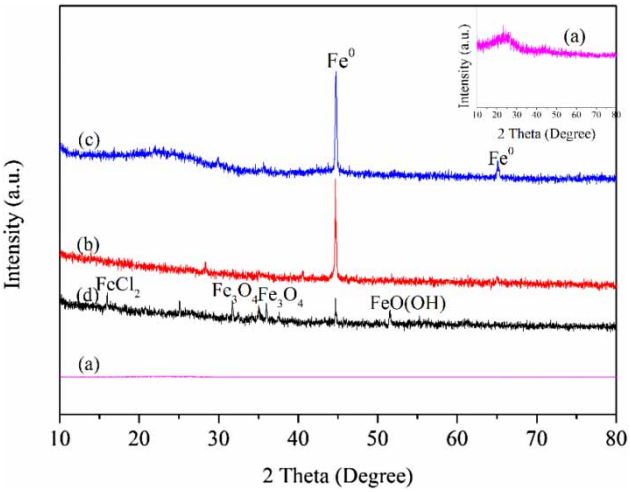

Figure 3 | XRD spectra of nZVI/SBC: (a) SBC, (b) 1ZVI/SBC, (c) 4ZVI/SBC, (d) 6ZVI/SBC.

The iron–biochar mass ratios of nZVI/SBC by using atomic absorption spectrophotometry were 0.081:1 (1ZVI/SBC), 0.132:1 (2ZVI/SBC), 0.275:1 (3ZVI/SBC), 0.52:1 (4ZVI/SBC), 2.68:1 (5ZVI/SBC) and 5.47:1 (6ZVI/SBC), respectively. The result data were consistent with the above experimental theoretical setting $FeCl_3{\cdot}6H_2O$/biomass impregnation mass ratio data. The removal efficiency of phenol increased rapidly with the increase in $FeCl_3{\cdot}6H_2O$/biomass impregnation mass ratio from 0.4 g/g to 2.7 g/g, but this trend was reversed at the higher ratios (above 2.7 g/g) in Figure 1. Fe^0 was consumed to generate ferrous iron as shown from Equations (9)–(11) (Yan *et al.* 2015), and ferrous iron activated persulfate through Equation (12). Increasing $FeCl_3{\cdot}6H_2O$/biomass impregnation mass ratios of 0.4 g/g (1ZVI/SBC) to 2.7 g/g (4ZVI/SBC) yielded more $SO_4^{\cdot-}$ species according to Equation (12) that accelerated the decomposition of phenol. The removal efficiency of phenol by added 5ZVI/SBC or 6ZVI/SBC was lower than by the addition of 4ZVI/SBC. One reason was that the excess of Fe^{2+} could be reacted with $SO_4^{\cdot-}$ to generate SO_4^{2-} (Equation (13)) (Anipsitakis & Dionysiou 2004) resulting in the disappearance of $SO_4^{\cdot-}$ species that resulted in the lower removal efficiency of phenol. Another reason may be that the $SO_4^{\cdot-}$ species scavenged persulfate radicals via Equations (14) and (15) (Yan *et al.* 2015) and thus decreased the observed efficiency of persulfate in degrading phenol. Hence, 4ZVI/SBC with the optimum $FeCl_3{\cdot}6H_2O$/biomass impregnation mass ratio of 2.7 g/g acted as the best activator of persulfate for phenol degradation. In addition, the mass of the dissolved iron of 4ZVI/SBC into solution accounts for 0.8 wt.% of the total mass of 4ZVI/SBC. The recovery of zerovalent-iron–biochar after reaction can be realized with the small amount of dissolved iron in the water:

$$2Fe^0 + O_2 + 2H_2O \rightarrow 2Fe^{2+} + 4OH^- \quad (9)$$

$$Fe^0 + 2H_2O \rightarrow Fe^{2+} + 2OH^- + H_2 \quad (10)$$

$$Fe^0 + S_2O_8^{2-} \rightarrow Fe^{2+} + 2SO_4^{2-} \quad (11)$$

$$Fe^{2+} + S_2O_8^{2-} \rightarrow Fe^{3+} + SO_4^{\cdot-} + SO_4^{2-} \quad (12)$$

$$SO_4^{\cdot-} + Fe^{2+} \rightarrow Fe^{3+} + SO_4^{2-} \quad (13)$$

$$SO_4^{\cdot-} + SO_4^{\cdot-} \rightarrow S_2O_8^{2-} \quad (14)$$

$$SO_4^{\cdot-} + S_2O_8^{2-} \rightarrow SO_4^{2-} + S_2O_8^{\cdot-} \quad (15)$$

Specific surface area and pore distribution of nZVI/SBC were determined by N_2 adsorption–desorption (Table 1). As can be observed, 1ZVI/SBC had a specific surface area of 220.93 $m^2{\cdot}g^{-1}$ and a total pore volume of 156.95×10^{-3} $cm^3{\cdot}g^{-1}$. The pore diameter measured was 1.42 nm for 1ZVI/SBC (below 2.0 nm) thus indicating micro-pores (Leng *et al.* 2015), and hence could limit the incorporation of the phenol molecules into the pores.

Table 1 | N_2 adsorption–desorption characterization of nZVI/SBC

Entry	Specific surface area ($m^2 \cdot g^{-1}$)	Total pore volume ($cm^3 \cdot g^{-1}$) $\times 10^{-3}$	Pore volume ($cm^3 \cdot g^{-1}$) $\times 10^{-3}$	Pore diameter (nm)
SBC	35.24	53.21	15.28	3.02
1ZVI/SBC	220.93	156.95	106.89	1.42
4ZVI/SBC	78.67	231.64	35.19	5.89
6ZVI/SBC	11.88	96.67	5.34	16.27

In contrast, 4ZVI/SBC and 6ZVI/SBC were mesopore materials according to the classification method recommended by IUPAC (Wang *et al.* 2017). It is worthwhile to note that the specific surface area (78.67 $m^2 \cdot g^{-1}$), pore diameter (5.89 nm) and total pore volume (231.64×10^{-3} $cm^3 \cdot g^{-1}$) of 4ZVI/SBC are larger than these of 6ZVI/SBC, benefiting the adsorption of phenol on the surface. The result is consistent with the phenol degradation results that 4ZVI/SBC was the best activator of persulfate for phenol degradation (versus 5ZVI/SBC and 6ZVI/SBC).

Razmi *et al.* (2017) successively removed phenol from wastewater using biochar-La as an activator to activate persulfate for phenol degradation. The specific surface area of biochar-La was 31.2 $m^2 \cdot g^{-1}$. The specific surface area of bentonite-supported nanoscale zerovalent iron used by Diao *et al.* (2016) for the removal of phenol was 39.41 $m^2 \cdot g^{-1}$. However, the specific surface area of these reported activators was lower than that of the 4ZVI/SBC activator in the paper, and the higher surface area of 4ZVI/SBC increased the ability to activate persulfate. Rahmani *et al.* (2018) demonstrated 93.98% removal of phenol with chelating agent Fe^0/complex as the activated persulfate material. The phenol removal percentage was 91% employing biochar modified with iron support as a catalyst (Liu *et al.* 2017). Nguyen & Oh (2019) studied the degradation efficiency of phenol maximized up to 97% in an Fe(0)–biochar–persulfate system after 330 min. Relative to the past literature, the one-step synthesis of zerovalent-iron–biochar composites in our work activates persulfate for phenol degradation with high efficiency (95.65% for 30 min at 25 °C).

Effect of 4ZVI/SBC dosage on phenol degradation

The effect of 4ZVI/SBC dosage on the activation of persulfate for phenol degradation is shown in Figure 4. The removal efficiency of phenol increased from 37.55% at 0.1 $g \cdot L^{-1}$ to 95.65% at 0.5 $g \cdot L^{-1}$ of 4ZVI/SBC. This trend can be attributed to the fact that more $SO_4^{\cdot-}$ species are yielded with the increasing of the dosage of 4ZVI/SBC which then accelerates the decomposition of phenol. At the same time, this could be due to an increase in the 4ZVI/SBC dosage accelerating the presence of additional redox-active centers and the presence of a sufficient quantity of iron species, which serve as electron donors. However, if the 4ZVI/SBC dosage was excessive, and the excessive Fe^{2+} consumed and scavenged $SO_4^{\cdot-}$ through electron transfer reactions, then a reducing reaction efficiency may be observed (Dong *et al.* 2017). From the above tests, we determined that the reasonable 4ZVI/SBC dosage was 0.5 $g \cdot L^{-1}$.

Effect of inorganic ions on phenol degradation

The generated $SO_4^{\cdot-}$ can be scavenged by inorganic ions such as Cl^-, SO_4^{2-} and NO_3^- (Epold *et al.* 2015). Figure 5 shows that the inorganic ions of Cl^-, SO_4^{2-} and NO_3^- affected the removal efficiency of phenol with the addition of 4ZVI/SBC as an activator. The removal efficiency of phenol without interfering ions was higher than that with the addition of interfering ions as the reaction time proceeded. It was observed that 86.12%, 82.58% and 71.08% of phenol removal efficiency occurred with the appearance of Cl^-, SO_4^{2-} and NO_3^- for 30 min, respectively.

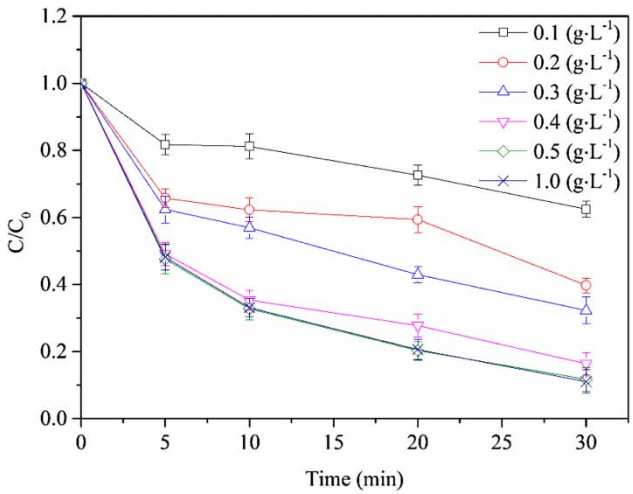

Figure 4 | Effect of 4ZVI/SBC dosage on the activation of persulfate for phenol degradation.

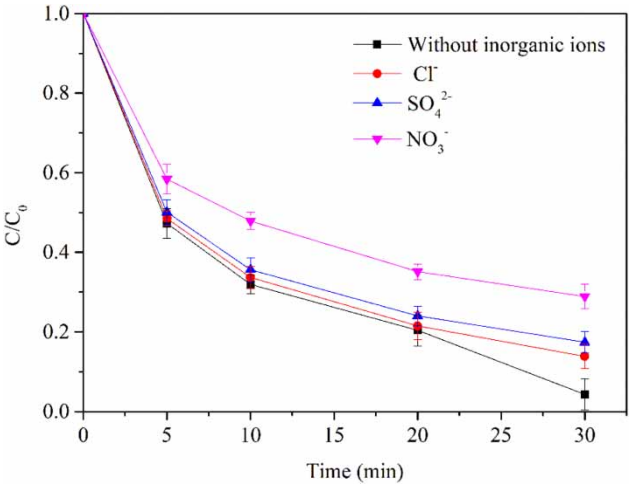

Figure 5 | Effect of inorganic ions on the activation of persulfate for phenol degradation.

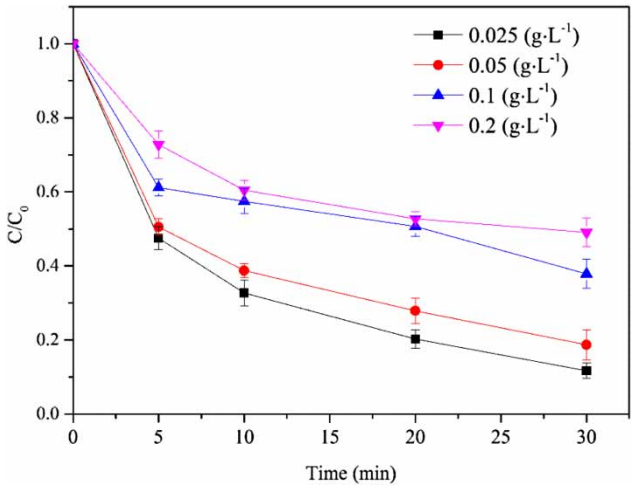

Figure 6 | Effect of phenol concentration on the activation of persulfate for phenol degradation.

The reason for this was that the adsorption rate of Cl^-, SO_4^{2-} and NO_3^- was higher than that of phenol molecules on the surface of 4ZVI/SBC, hence leading to the decreased phenol removal efficiency (Epold *et al.* 2015). Cl^- and SO_4^{2-} have no significant impact on phenol degradation, but NO_3^- has a negative impact on phenol degradation. The inhibition removal efficiency of phenol by adding SO_4^{2-} was small and likely resulted from the formation of inner-sphere complexes on the 4ZVI/SBC surface by SO_4^{2-} (Li *et al.* 2017). Cl^- has little impact on inhibition of phenol degradation because Cl^- reacts with $SO_4^{\cdot-}$ to produce $Cl^{\cdot}$ and SO_4^{2-} following Equation (16) (Rahmani *et al.* 2018). NO_3^- exhibited the strongest inhibitive effect on phenol degradation because the presence of NO_3^- was the competition with persulfate for reactive sites on the 4ZVI/SBC surface (Wang *et al.* 2013). Another reason may be that the NO_3^- acts as a scavenger for sulfate-free radicals (Equation (17)) (Wang *et al.* 2013):

$$SO_4^{\cdot-} + Cl^- \rightarrow Cl^{\cdot} + SO_4^{2-} \quad (16)$$

$$SO_4^{\bullet-} + NO_3^- \rightarrow NO_3^{\bullet} + SO_4^{2-} \quad (17)$$

Effect of phenol concentration on phenol degradation

The effect of phenol concentration on the activation of persulfate for phenol degradation was also investigated, as shown in Figure 6. As can be observed from Table 2, the phenol concentration affected the first-order kinetic rate constant and the removal efficiency of phenol. As the concentration of phenol was increased from 0.025 to 0.2 g·L^{-1}, a drastic reduction of the phenol removal efficiency was observed. It is worth noting that as the phenol concentration was increased, the

Table 2 | The first-order kinetic rate constant and the removal efficiency of phenol with different phenol concentrations

Entry	[phenol] (g·L^{-1})	[4ZVI/SBC] (g·L^{-1})	Removal efficiency of phenol (%)	The first-order kinetic rate constant	
				K_1·min^{-1}	R^2
1	0.025	0.5	95.65	0.09510	0.95639
2	0.05	0.5	87.31	0.06160	0.95151
3	0.1	0.5	62.15	0.02703	0.84799
4	0.2	0.5	50.90	0.02518	0.82927

active sites of the 4ZVI/SBC surface were largely occupied which then resulted in the decrease of the removal efficiency of phenol. One possibility is that $SO_4^{\cdot-}$ reacts with H_2O to produce OH· (Equation (18)) which then forms $Fe(OH)_3$ precipitation (Wang *et al.* 2013) on the surface of the 4ZVI/SBC thus preventing the degradation of phenol by iron species:

$$SO_4^{\cdot-} + H_2O \rightarrow SO_4^{2-} + OH^{\cdot} + H^+ \quad (18)$$

Phenol and persulfate take place on the adjacent vacant surfaces at the solid–liquid interface according to the Langmuir–Hinshelwood mechanism in heterogeneous catalysis systems, and the surface reaction of adsorbed species is the first reaction step (Rao *et al.* 2018). The initial rate (r_0) can be expressed as (Rao *et al.* 2018):

$$r_0 = -\frac{dC_0}{dt} = \frac{kKC_0}{1 + KC_0} \quad (19)$$

$$r_0 = -\frac{dC_0}{dt} = K_1 C_0 \quad (20)$$

where C_0 is the initial concentration of phenol, K is the equilibrium adsorption constant of phenol on the 4ZVI/SBC surface (mM^{-1}), k represents the limiting reaction rate at maximum coverage in this system ($mM \cdot min^{-1}$), and K_1 is the first-order kinetic rate constant.

Equations (19) and (20) are connected to Equation (21); k and K were decided to be 0.06325 $mM \cdot min^{-1}$ and 1.56299 mM^{-1} from the slope and intercept, respectively:

$$\frac{1}{K_1} = \frac{1}{k}C_0 + \frac{1}{kK} \tag{21}$$

Effect of pH on phenol degradation

The pH is a key factor in wastewater chemical treatment processes (Rahmani *et al.* 2017). The effect of pH on the activation of persulfate for phenol degradation by the addition of 4ZVI/SBC activator is shown in Figure 7. From Table 3, we can observe that pH affected the first-order kinetic rate constant, the initial concentration of phenol reduction and the removal efficiency of phenol. A 97.40% removal efficiency of phenol could be achieved at pH of 3.09, while, 89.97%, 92.92%, 88.30% and 78.66% of phenol removal efficiency were achieved at pH of 5.04, 6.86, 9.06 and 11.03, respectively. The optimal removal efficiency of phenol and first-order kinetic rate constant were observed at a pH of 3.09. According to Equations (22) and (23) (Liang *et al.* 2007), the breakdown of persulfate into $SO_4^{\cdot-}$ can occur under acidic conditions which can then produce a rapid attack on phenol. In this case, the oxygen reactions with zerovalent iron under acidic conditions are also a factor in forming ferrous iron production according to Equations (24) and (25) (Matzek & Carter 2017). According to Equation (26), zerovalent iron was also corroded into ferric iron under acidic pH conditions, and ferric iron reacted with zerovalent iron to produce ferrous ions (Matzek & Carter 2017). More ferrous iron is made available to generate sulfate radicals. Because $SO_4^{\cdot-}$ was the main radical in acidic solution (Yan *et al.* 2015), the removal efficiency of phenol under acidic conditions was higher than that under alkaline conditions. The removal efficiency of phenol decreased with an increased pH (pH > 6.86). The generated $SO_4^{\cdot-}$ reacted with OH^- to produce $HSO_4^{\cdot-}$ under alkaline conditions according to Equations (27) and (28) (Rahmani *et al.* 2018). The removal efficiency of phenol decreased because of the decomposition of sulfate and hydroxyl radicals. Another reason may be that the precipitation of ferric iron forms oxyhydroxides like $FeOH^{2+}$/$Fe(OH)^{2+}$ on the 4ZVI/SBC activator surface that inhibit activating persulfate to form $SO_4^{\cdot-}$ in alkaline conditions (Xia *et al.* 2017). Therefore, it is evident that pH affected the activity of persulfate and the oxidation mechanism of the reaction:

Table 3 | The first-order kinetic rate constant and the efficiency of phenol degradation with different pH

Entry	[4ZVI/SBC] ($g \cdot L^{-1}$)	pH	Removal efficiency of phenol (%)	The first-order kinetic rate constant	
				$K_1 \cdot min^{-1}$	R^2
1	0.5	3.09	97.40	0.10402	0.93698
2	0.5	5.04	89.97	0.06387	0.90479
3	0.5	6.86	92.92	0.08102	0.97611
4	0.5	9.06	88.30	0.06611	0.96106
5	0.5	11.03	78.66	0.04203	0.83830

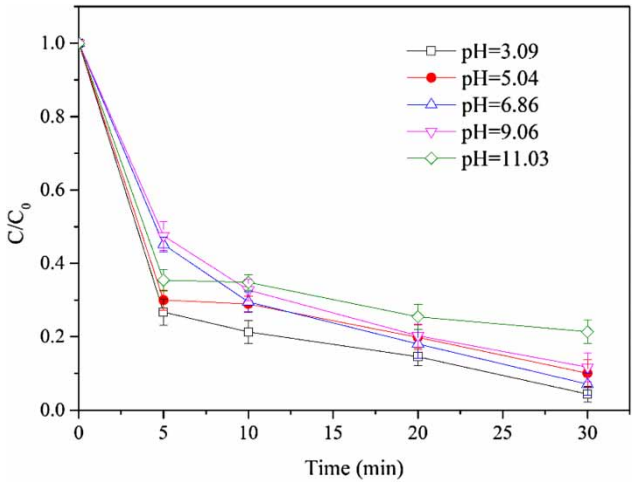

Figure 7 | Effect of pH on the activation of persulfate for phenol degradation.

$$S_2O_8^{2-} + H^+ \rightarrow HS_2O_8^- \tag{22}$$

$$HS_2O_8^- \rightarrow SO_4^{\cdot-} + SO_4^{2-} + H^+ \tag{23}$$

$$2Fe^0 + O_2 + 4H^+ \rightarrow 2Fe^{2+} + 2H_2O \tag{24}$$

$$2Fe^0 + 2O_2 + 4H^+ \rightarrow 2Fe^{2+} + 2H_2O_2 \tag{25}$$

$$Fe^0 + 2Fe^{3+} \rightarrow 3Fe^{2+} \tag{26}$$

$$SO_4^{\cdot-} + OH^- \rightarrow OH^{\cdot} + SO_4^{2-} \tag{27}$$

$$OH^{\cdot} + SO_4^{2-} \rightarrow HSO_4^{\cdot-} + 0.5O_2 \tag{28}$$

The adsorption of phenol can be described by the Langmuir–Hinshelwood mechanism, assuming that phenol

Table 4 | Effect of the ozonation time on the removal of phenol and COD concentration

Time/min	0	15	30
Phenol concentration ($\times10^{-3}$ g·L^{-1})	25	4.02	1.09
Removal efficiency of phenol (%)	0	83.91	95.65
COD concentration ($\times10^{-3}$ g·L^{-1})	128	36.00	5.58
Removal efficiency of COD (%)	0	72.81	95.64

and H^+ compete with the reacting substrate for the active surface sites on 4ZVI/SBC at different pH. Equation (29) may be written as by Theurich and co-workers (Theurich *et al.* 1996). Equations (29) and (20) are connected to calculate a k_1 of 0.054 mM·min^{-1}. The pH affects the limiting reaction rate at maximum coverage of phenol:

$$r_0 = -\frac{dC_0}{dt} = \frac{k_1 K C_0}{1 + K C_0 + K_{H^+} C_{H^+}} \quad (29)$$

where C_0 is the initial concentration of phenol, K is the equilibrium adsorption constant of phenol on the 4ZVI/SBC surface (mM^{-1}), k_1 represents the limiting reaction rate at maximum coverage in this system (mM·min^{-1}), K_{H^+} is the adsorption coefficient, and C_{H^+} is the concentration of H^+.

Verification of the oxidation result for phenol

The theoretical oxygen demand for the oxidation of phenol to CO_2 is an obligatory (Contreras *et al.* 2011) parameter that must be measured. The concentration of phenol and COD in the aqueous phase were measured as a function of time to confirm the reliability of the proposed methods. From Table 4 we can observe that the trend of phenol and COD concentration changed in the aqueous phase at different time periods. The removal efficiency of phenol increased from 83.91% at 15 min to 95.65% at 30 min, while the removal efficiency of COD values increased from 72.81% at 15 min to 95.64% at 30 min. The results revealed that COD concentration values decreased with the decrease of phenol concentration in the solution, which indicated that phenol was degraded using the activated sodium persulfate by 4ZVI/SBC into non-toxic CO_2, H_2O, and other small molecular compounds.

CONCLUSIONS

The zerovalent-iron–biochar composite was synthesized via a one-step pyrolysis of $FeCl_3$-laden sorghum straw biomass and activated persulfate for phenol degradation. The structural information and composition of the nZVI/SBC were characterized by atomic absorption spectrophotometry, N_2 adsorption–desorption, SEM and XRD. The 4ZVI/SBC was a mesopore material with a specific surface area of 78.669 m^2·g^{-1}, a pore diameter of 5.89 nm and a total pore volume of 231.64×10^{-3} cm^3·g^{-1}, which benefitted the adsorption of phenol on its surface. The 4ZVI/SBC was mainly composed of Fe^0 with the best $FeCl_3{\cdot}6H_2O$/biomass impregnation mass ratio of 2.7 g/g. The removal efficiency of phenol increased with increased dosage of 4ZVI/SBC from 37.55% at 0.1 g·L^{-1} to 95.65% at 0.5 g·L^{-1}. The appearance of Cl^-, SO_4^{2-} and NO_3^- affected the removal efficiency of phenol with the addition of 4ZVI/SBC in the following order: $Cl^- < SO_4^{2-} < NO_3^-$. The optimal removal efficiency of phenol and first-order kinetic rate constant were observed at pH 3.09. The results showed that phenol was successfully transformed into CO_2 and H_2O in the presence of 4ZVI/SBC activator with a small amount of dissolved iron in the water. The one-step preparation method of 4ZVI/SBC exhibited satisfactory activation of persulfate for phenol degradation that may be used as an alternative eco-friendly methodology.

ACKNOWLEDGEMENTS

This project was supported by the National Key Research and Development Program of China (2017YFD0800301) and the National Natural Science Foundation of China (Grant Nos. 41373127, 41703129 and 41773136).

REFERENCES

Anipsitakis, G. P. & Dionysiou, D. D. 2004 Radical generation by the interaction of transition metals with common oxidants. *Environmental Science & Technology* **38** (13), 3705–3712.

Chen, W., Pan, X. L. & Bao, X. H. 2007 Tuning of redox properties of iron and iron oxides via encapsulation within carbon nanotubes. *Journal of the American Chemical Society* **129** (23), 7421–7426.

Contreras, E. M., Bertola, N. C. & Zaritzky, N. E. 2011 Monitoring the ozonation of phenol solutions at constant pH by different methods. *Industrial & Engineering Chemistry Research* **50** (16), 9799–9809.

Devi, P. & Saroha, A. K. 2014 Synthesis of the magnetic biochar composites for use as an adsorbent for the removal of pentachlorophenol from the effluent. *Bioresource Technology* **169**, 525–531.

Diao, Z. H., Xu, X. R., Jiang, D., Kong, L. J., Sun, Y. X., Hu, Y. X., Hao, Q. W. & Chen, H. 2016 Bentonite-supported nanoscale

zero-valent iron/persulfate system for the simultaneous removal of Cr(VI) and phenol from aqueous solutions. *Chemical Engineering Journal* **302**, 213–222.

Dong, C. D., Chen, C. W. & Hung, C. M. 2017 Synthesis of magnetic biochar from bamboo biomass to activate persulfate for the removal of polycyclic aromatic hydrocarbons in marine sediments. *Bioresource Technology* **245** (A), 188–195.

Duan, X., Ao, Z., Li, D., Sun, H., Zhou, L., Suvorova, A., Saunders, M., Wang, G. & Wang, S. 2016 Surface-tailored nanodiamonds as excellent metal-free catalysts for organic oxidation. *Carbon* **103**, 404–411.

Duan, X., Sun, H. & Wang, S. 2018 Metal-free carbocatalysis in advanced oxidation reactions. *Accounts of Chemical Research* **51** (3), 678–687.

Epold, I., Trapido, M. & Dulova, N. 2015 Degradation of levofloxacin in aqueous solutions by Fenton, ferrous ion-activated persulfate and combined Fenton/persulfate systems. *Chemical Engineering Journal* **279**, 452–462.

Fang, G., Chen, X., Wu, W., Liu, C., Dionysiou, D. D., Fan, T., Wang, Y., Zhu, C. & Zhou, D. 2018 Mechanisms of interaction between persulfate and soil constituents: activation, free radical formation, conversion, and identification. *Environmental Science & Technology* **52** (24), 14352–14361.

Hsueh, Y. H., Tsai, P. H., Lin, K. S., Ke, W. J. & Chiang, C. L. 2017 Antimicrobial effects of zero-valent iron nanoparticles on Gram-positive *Bacillus* strains and Gram-negative *Escherichia coli* strains. *Journal of Nanobiotechnology* **15**, 77.

Huggins, T. M., Haeger, A., Biffinger, J. C. & Ren, Z. J. 2016 Granular biochar compared with activated carbon for wastewater treatment and resource recovery. *Water Research* **94**, 225–232.

Jung, K. W., Choi, B. H., Jeong, T. U. & Ahn, K. H. 2016 Facile synthesis of magnetic biochar/Fe_3O_4 nanocomposites using electro-magnetization technique and its application on the removal of acid orange 7 from aqueous media. *Bioresource Technology* **220**, 672–676.

Kim, C., Ahn, J. Y., Kim, T. Y., Shin, W. S. & Hwang, I. 2018 Activation of persulfate by nanosized zero-valent iron (NZVI): mechanisms and transformation products of NZVI. *Environmental Science & Technology* **52** (6), 3625–3633.

Lee, H., Kim, H. I., Weon, S., Choi, W., Hwang, Y. S., Seo, J., Lee, C. & Kim, J. H. 2016 Activation of persulfates by graphitized nanodiamonds for removal of organic compounds. *Environmental Science & Technology* **50** (18), 10134–10142.

Lei, Y., Chen, C. S., Tu, Y. J., Huang, Y. H. & Zhang, H. 2015 Heterogeneous degradation of organic pollutants by persulfate activated by CuO-Fe_3O_4: mechanism, stability, and effects of pH and bicarbonate ions. *Environmental Science & Technology* **49** (11), 6838–6845.

Leng, L. J., Yuan, X. Z., Huang, H. J., Wang, H., Wu, Z. B., Fu, L. H., Peng, X., Chen, X. H. & Zeng, G. M. 2015 Characterization and application of bio-chars from liquefaction of microalgae, lignocellulosic biomass and sewage sludge. *Fuel Processing Technology* **129**, 8–14.

Li, H., Chen, Y. Q., Chen, S., Wang, X. L., Guo, S., Qiu, Y. F., Liu, Y. D., Duan, X. L. & Yu, Y. J. 2017 Wheat straw biochar-supported nanoscale zerovalent iron for removal of trichloroethylene from groundwater. *PLoS ONE* **12** (3), e0172337.

Liang, C. J., Wang, Z. S. & Bruell, C. J. 2007 Influence of pH on persulfate oxidation of TCE at ambient temperatures. *Chemosphere* **66** (1), 106–113.

Lisowski, P., Colmenares, J. C., Mašek, O., Lisowski, W., Lisovytskiy, D., Kamińska, A. & Łomot, D. 2017 Dual functionality of TiO_2/biochar hybrid materials: photocatalytic phenol degradation in the liquid phase and selective oxidation of methanol in the gas phase. *ACS Sustainable Chemistry & Engineering* **5** (7), 6274–6287.

Liu, W. J., Tian, K., Jiang, H. & Yu, H. Q. 2013 Facile synthesis of highly efficient and recyclable magnetic solid acid from biomass waste. *Scientific Reports* **3**, 2419.

Liu, X., Yin, H., Lin, A. & Guo, Z. 2017 Effective removal of phenol by using activated carbon supported iron prepared under microwave irradiation as a reusable heterogeneous Fenton-like catalyst. *Journal of Environmental Chemical Engineering* **5** (1), 870–876.

Matzek, L. W. & Carter, K. E. 2017 Sustained persulfate activation using solid iron: kinetics and application to ciprofloxacin degradation. *Chemical Engineering Journal* **307**, 650–660.

Nguyen, T. A. & Oh, S. Y. 2019 Biochar-mediated oxidation of phenol by persulfate activated with zero-valent iron. *Journal of Chemical Technology & Biotechnology* **94** (12), 3932–3940.

Oh, S. Y., Seo, Y. D., Ryu, K. S., Park, D. J. & Lee, S. H. 2017 Redox and catalytic properties of biochar-coated zero-valent iron for the removal of nitro explosives and halogenated phenols. *Environmental Science: Processes & Impacts* **19** (5), 711–719.

Pu, M., Ma, Y., Wan, J., Wang, Y., Huang, M. & Chen, Y. 2014 Fe/S doped granular activated carbon as a highly active heterogeneous persulfate catalyst toward the degradation of Orange G and diethyl phthalate. *Journal of Colloid and Interface Science* **418**, 330–337.

Rahmani, A. R., Rezaei-Vahidian, H., Almasi, H. & Donyagard, F. 2017 Modeling and optimization of ciprofloxacin degradation by hybridized potassium persulfate/zero valent-zinc/ultrasonic process. *Environmental Processes* **4** (3), 563–572.

Rahmani, A. R., Poormohammadi, A., Zamani, F., Birgani, Y. T., Jorfi, S., Gholizadeh, S., Mohammadi, M. J. & Almasi, H. 2018 Activated persulfate by chelating agent Fe/complex for in situ degradation of phenol: intermediate identification and optimization study. *Research on Chemical Intermediates* **44** (9), 5501–5519.

Rao, Y., Han, F., Chen, Q., Wang, D., Xue, D., Wang, H. & Pu, S. 2018 Efficient degradation of diclofenac by $LaFeO_3$-catalyzed peroxymonosulfate oxidation: kinetics and toxicity assessment. *Chemosphere* **218**, 299–307.

Razmi, R., Ramavandi, B., Ardjmand, M. & Heydarinasab, A. 2017 Efficient phenol removal from petrochemical wastewater using biochar-La/ultrasonic/persulphate system: characteristics, reusability, and kinetic study. *Environmental Technology* **40** (7), 822–834.

Su, Y. F., Cheng, Y. L. & Shih, Y. H. 2013 Removal of trichloroethylene by zerovalent iron/activated carbon derived from agricultural wastes. *Journal of Environmental Management* **129**, 361–366.

Sun, H., Zhou, G., Liu, S., Ang, H. M., Tadé, M. O. & Wang, S. 2012 Nano-Fe^0 encapsulated in microcarbon spheres: synthesis, characterization, and environmental applications. *ACS Applied Materials & Interfaces* **4** (11), 6235–6241.

Theurich, J., Lindner, M. & Bahnemann, D. W. 1996 Photocatalytic degradation of 4-chlorophenol in aerated aqueous titanium dioxide suspensions: a kinetic and mechanistic study. *Langmuir* **12** (26), 6368–6376.

Wang, T., Su, J., Jin, X., Chen, Z., Megharaj, M. & Naidu, R. 2013 Functional clay supported bimetallic nZVI/Pd nanoparticles used for removal of methyl orange from aqueous solution. *Journal of Hazardous Materials* **262** (22), 819–825.

Wang, J., Liao, Z., Ifthikar, J., Shi, L., Du, Y., Zhu, J., Xi, S., Chen, Z. & Chen, Z. 2017 Treatment of refractory contaminants by sludge-derived biochar/persulfate system via both adsorption and advanced oxidation process. *Chemosphere* **185**, 754–763.

Wu, S., He, H., Li, X., Yang, C., Zeng, G., Wu, B., He, S. & Lu, L. 2018 Insights into atrazine degradation by persulfate activation using composite of nanoscale zero-valent iron and graphene: performances and mechanisms. *Chemical Engineering Journal* **341**, 126–136.

Xia, D., Yin, R., Sun, J., An, T., Li, G., Wang, W., Zhao, H. & Wong, P. K. 2017 Natural magnetic pyrrhotite as a high-efficient persulfate activator for micropollutants degradation: radicals identification and toxicity evaluation. *Journal of Hazardous Materials* **340**, 435–444.

Yan, J., Lei, M., Zhu, L., Anjum, M. N., Zou, J. & Tang, H. 2011 Degradation of sulfamonomethoxine with Fe_3O_4 magnetic nanoparticles as heterogeneous activator of persulfate. *Journal of Hazardous Materials* **186** (2–3), 1398–1404.

Yan, J., Han, L., Gao, W., Xue, S. & Chen, M. 2015 Biochar supported nanoscale zerovalent iron composite used as persulfate activator for removing trichloroethylene. *Bioresource Technology* **175**, 269–274.

Yang, S. Y., Yang, X., Shao, X. T., Niu, R. & Wang, L. L. 2011 Activated carbon catalyzed persulfate oxidation of azo dye acid orange 7 at ambient temperature. *Journal of Hazardous Materials* **186** (1), 659–666.

Yang, J., Zhao, Y., Ma, S., Zhu, B., Zhang, J. & Zheng, C. 2016 Mercury removal by magnetic biochar derived from simultaneous activation and magnetization of sawdust. *Environmental Science & Technology* **50** (21), 12040–12047.

Zhou, Y., Gao, B., Zimmerman, A. R., Chen, H., Zhang, M. & Cao, X. 2014 Biochar-supported zerovalent iron for removal of various contaminants from aqueous solutions. *Bioresource Technology* **152**, 538–542.

First received 16 August 2019; accepted in revised form 19 December 2019. Available online 2 January 2020